



# Seasonal Distributions of Methane in a Populous Urban Coastal Sea Area

Hsiao-Chun Tseng<sup>1,2\*</sup>, Chia-Chia Lin<sup>1</sup>, Hui-Juan Pan<sup>3</sup>, Yokie Tai Yuh Han<sup>1</sup>  
and Gwo-Ching Gong<sup>1,2\*</sup>

<sup>1</sup> Institute of Marine Environment and Ecology, National Taiwan Ocean University, Keelung, Taiwan, <sup>2</sup> Center of Excellence for the Oceans, National Taiwan Ocean University, Keelung, Taiwan, <sup>3</sup> Institute of Earth Sciences, College of Ocean Science and Resource, National Taiwan Ocean University, Keelung, Taiwan

## OPEN ACCESS

### Edited by:

William Savidge,  
Odum School of Ecology,  
University of Georgia, United States

### Reviewed by:

Stefano Bonaglia,  
University of Gothenburg, Sweden  
Masahiro Suzumura,  
National Institute of Advanced  
Industrial Science and Technology  
(AIST), Japan

### \*Correspondence:

Hsiao-Chun Tseng  
h.c.jean.tseng@gmail.com  
Gwo-Ching Gong  
gcong@mail.ntou.edu.tw

### Specialty section:

This article was submitted to  
Coastal Ocean Processes,  
a section of the journal  
Frontiers in Marine Science

Received: 26 December 2021

Accepted: 02 March 2022

Published: 07 April 2022

### Citation:

Tseng H-C, Lin C-C, Pan H-J,  
Han YTY and Gong G-C (2022)  
Seasonal Distributions of Methane in a  
Populous Urban Coastal Sea Area.  
Front. Mar. Sci. 9:843549.  
doi: 10.3389/fmars.2022.843549

Methane (CH<sub>4</sub>) is an important greenhouse gas, and its concentrations in aquatic areas are heavily influenced by anthropogenic activities, especially human-induced eutrophication, polluted river discharge and wastewater treatment plant (WWTP) effluents. Although coastal areas and estuaries contribute large amounts of global oceanic CH<sub>4</sub> emissions, the relative contributions of different sources have not been well determined. The Tamsui River located in northern Taiwan is an urban river flowing through populated cities and thus likely carries large amounts of contaminants, such as nutrients and organic matter to the estuary. In this study, we characterized the spatial distribution and seasonal variations in CH<sub>4</sub> in the Tamsui River estuary adjacent marine areas. The sea-to-air CH<sub>4</sub> fluxes were also estimated to quantify the strength of the study area as an atmospheric CH<sub>4</sub> source. Our results showed that CH<sub>4</sub> concentrations in coastal sea areas were influenced by WWTP effluents, sediment and freshwater inputs. Thus, river discharge and nutrient levels as well as strong vertical mixing and disturbances might increase CH<sub>4</sub> concentrations and emissions. The seasonal surface CH<sub>4</sub> concentrations and sea-to-air CH<sub>4</sub> fluxes were 13.7 ± 18.7 nM and 41.7 ± 68.0 μmol m<sup>-2</sup> d<sup>-1</sup> in autumn; 29.3 ± 19.8 nM and 61.3 ± 44.6 μmol m<sup>-2</sup> d<sup>-1</sup> in spring; 21.8 ± 13.9 nM and 37.0 ± 26.2 μmol m<sup>-2</sup> d<sup>-1</sup> in summer; and 27.0 ± 21.4 nM and 85.9 ± 75.4 μmol m<sup>-2</sup> d<sup>-1</sup> in winter.

**Keywords:** methane, WWTP effluents, nutrients, Tamsui River, greenhouse gases

## INTRODUCTION

Methane (CH<sub>4</sub>), the second most important greenhouse gas after carbon dioxide (CO<sub>2</sub>), has global warming potential over a 20-year time frame (GWP<sub>20</sub>) that is 86 times as high as that of CO<sub>2</sub> (IPCC, 2013). It accounts for 16–25% of atmospheric warming to date (Etminan et al., 2016). The global atmospheric CH<sub>4</sub> concentration has increased significantly from a preindustrial value of 722 ± 25 ppb in 1750 to 1803 ± 2 ppb in 2011, and the most plausible cause of the increase in CH<sub>4</sub> concentration is human activities (IPCC, 2013). Kirschke et al. (2013) estimated that the global surface-to-air CH<sub>4</sub> emissions from 2000 to 2009 were 678 Tg CH<sub>4</sub> yr<sup>-1</sup>, with a large range of 542–852 Tg CH<sub>4</sub> yr<sup>-1</sup>. Jackson et al. (2020) also reported that the average global CH<sub>4</sub> emissions for 2017 were 596 Tg CH<sub>4</sub> yr<sup>-1</sup>, with a range of 572–614 Tg CH<sub>4</sub> yr<sup>-1</sup>. The open ocean is a modest source of

CH<sub>4</sub> to the atmosphere at a rate of less than 2 Tg CH<sub>4</sub> yr<sup>-1</sup> (Rhee et al., 2009). A large fraction of marine-originated CH<sub>4</sub> in the atmosphere is produced in oxygenated surface waters that are oversaturated with CH<sub>4</sub> in relation to atmospheric equilibrium (Karl et al., 2008; Repeta et al., 2016), an unexplained phenomenon referred to as the marine methane paradox (Reeburgh, 2007; Repeta et al., 2016). Previous research has revealed that most CH<sub>4</sub> found in the euphotic zone was released during zooplankton grazing (de Angelis and Lee, 1994) or in anoxic microenvironments within zooplankton fecal pellets (Tilbrook and Karl, 1994). Recent research has determined that the formation of CH<sub>4</sub> in oxic environments can occur *via* methylphosphonate cycling (Karl et al., 2008) and by dimethylsulfide (DMS) cycling (Damm et al., 2010; Florez-Leiva et al., 2013; Zindler et al., 2013). Moreover, Bogard et al. (2014) suggested a possible link between CH<sub>4</sub> concentration and phytoplankton standing stock (i.e., chlorophyll *a*), which implies that factors influencing phytoplankton standing stock, such as grazing, nutrient availability and the physical structure of the water column, have a strong bearing on pelagic CH<sub>4</sub> dynamics.

Coastal regions are more intense sources of CH<sub>4</sub> to the atmosphere, which contribute approximately 75% of global oceanic CH<sub>4</sub> emissions (Bange et al., 1994). Continental shelves emit approximately 13 Tg CH<sub>4</sub> yr<sup>-1</sup> (Bange et al., 1994), whereas estuaries emit between 1 and 7 Tg CH<sub>4</sub> yr<sup>-1</sup> (Bange et al., 1994; Upstill-Goddard et al., 2000). The high CH<sub>4</sub> concentrations in the surface waters of continental shelves are due to direct CH<sub>4</sub> inputs from estuaries and sediments where methanogenesis is sustained by abundant organic matter sedimentation (Bange et al., 1994; Rehder et al., 1998; Upstill-Goddard et al., 2000; Middelburg et al., 2002; Borges et al., 2018). In addition, the impacts of human activities on coastal CH<sub>4</sub> emissions, such as dam construction (Chen et al., 2008), eutrophication (Beaulieu et al., 2019), wastewater discharge into coastal areas (Du et al., 2018), changes in hydrology (Pekel et al., 2016) and climate feedbacks, such as microbial responses to warming (Yvon-Durocher et al., 2014), are not well understood and have been poorly quantified. Beaulieu et al. (2019) and Nijman et al. (2021) also reported that future CH<sub>4</sub> emissions from lakes and impoundments worldwide may increase due to increases in nutrients and water temperature. Borges et al. (2018) also found that productivity and temperature are drivers to seasonal and spatial variations of dissolved methane in the Southern Bight of the North Sea. In addition, Myllykangas et al. (2019) addressed that eutrophication and climate change may accelerate CH<sub>4</sub> emissions from estuaries, causing positive feedbacks with global warming.

The scope of this study is to investigate seasonal distributions of methane in a populous urban coastal sea area. Estuaries transfer terrestrial matter and human impacts (nutrients, organic matter etc.) from land to ocean. The Tamsui River is a populous urban river, and the highest regional population density in its catchment reaches 38,607 people per km<sup>2</sup> (Yonghe district). Recent research (Borges et al., 2016; Gelesh et al., 2016; Borges et al., 2018; Humborg et al., 2019) has found massive CH<sub>4</sub> emissions in estuaries and coastal water during

summertime, which might be due to temperature controlling methanogenesis in organic matter rich sediments. Since the seawater temperature was higher in tropical/subtropical areas than in temperate regions, the CH<sub>4</sub> concentrations in the water might also be higher, especially under future climate change. Seasonal data collection is needed for a comprehensive view of the situation. This research aims to understand the seasonal variations in CH<sub>4</sub> concentrations as well as their interaction with other environmental factors that may be influenced by human activities in a populous urban coastal area.

## MATERIALS AND METHODS

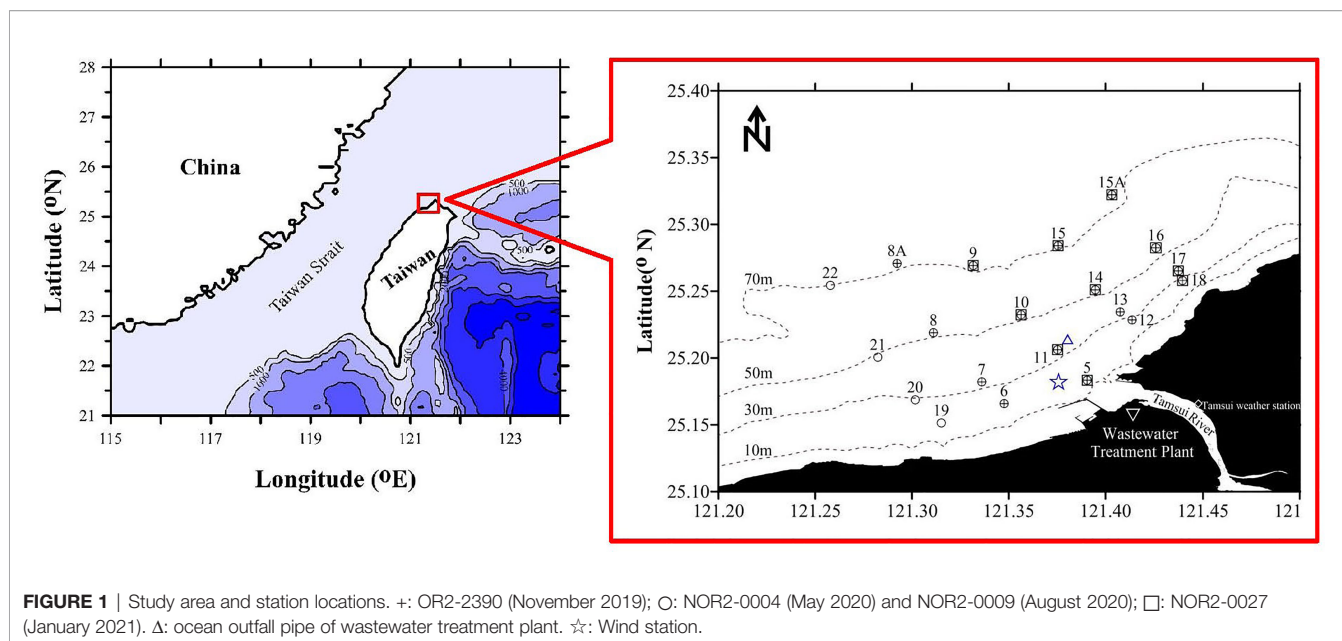
### Study Area

The Tamsui River is located in northern Taiwan (**Figure 1**) and has a total length of 159 km. The catchment area of the Tamsui River is 2,726 km<sup>2</sup>, and it covers the whole metropolitan area of Taipei, the capital city of Taiwan. The drainage basin includes several regions along the main tributaries where large amounts of nutrients, resulting from industrial and agricultural activities, enter the river (Wen et al., 2008). The Tamsui River delivers materials, including suspended particles, nutrients, organic matter, and pollutants, from land into its estuary and adjacent marine areas. There were 7.13 million people living in the catchment, and approximately 60% of the population utilized the sanitary sewers in 2019 (Tseng et al., 2021). The largest wastewater treatment plant (WWTP) in Taiwan is located near the Tamsui River estuary (**Figure 1**), and its ocean outfall pipe extends from the shore and enters the ocean. The outlet of the ocean outfall pipe of the WWTP was located near sampling station 11 (**Figure 1**) and its diffuser tubes are 3 km from shore at water depths between 30 m and 40 m.

The regional climate is subtropical, with temperatures varying between 10 and 35 °C and annual precipitation ranging between 1500 and 2500 mm (Wen et al., 2008). The dry season ranges from November to April, and the wet season ranges from May to October. According to the historical data from the Tamsui weather station (**Figure 1**) over the past 25 years (1995–2020), the average rainfall is 776 ± 269 mm during the dry season, while it is 1322 ± 440 mm during the wet season (Central Weather Bureau: <https://www.cwb.gov.tw/eng/>).

### Cruise Information and Sampling Instruments

Seasonal samples were taken in the Tamsui River estuary adjacent sea area (**Figure 1**) during four cruises onboard R/V Ocean Researcher 2 and R/V New Ocean Researcher 2: OR2-2390 (November 2019), NOR2-0004 (May 2020), NOR2-0009 (August 2020), and NOR2-0027 (January 2021). Discrete water samples were taken at various depths at 16 sampling stations in autumn (November 2019) and 20 sampling stations in spring (May 2020) and summer (August 2020). Due to the adverse weather conditions in winter (January 2021), discrete water samples were taken at various depths at 6 sampling stations, and surface water samples were taken at 10 sampling stations.



The vertical profiles of seawater temperature and salinity were measured with a conductivity–temperature–depth instrument (CTD; SBE 9/11, Seabird Scientific, USA). Seawater samples from various depths were collected using a carousel water sampler (SBE32, Seabird Scientific, USA) that was fitted with 20 L Teflon-coated Go-Flo bottles (General Oceanic, USA) mounted on a CTD assembly.

## Chemical Analysis

Water samples for nutrient analysis were placed in 100 mL polypropylene bottles and immediately frozen with liquid nitrogen. The methods employed for nitrate ( $\text{NO}_3^-$ ) and phosphate  $\text{PO}_4^{3-}$  analysis are described in detail elsewhere (Gong et al., 1996; Gong et al., 2000), and the precision was  $\pm 0.3$  and  $\pm 0.01 \mu\text{mol L}^{-1}$ , respectively. Dissolved oxygen (DO) was measured by spectrophotometry (Pai et al., 1993) with a precision of approximately  $\pm 0.32\%$  at the  $190 \mu\text{mol L}^{-1}$  level. Water samples for chlorophyll *a* (Chl *a*) analysis were immediately filtered through GF/F filter paper (Whatman, 47 mm) and stored at  $-20^\circ\text{C}$ . A Turner Designs model 10-AU-005 fluorometer (Turner Inc., USA) was utilized to measure the Chl *a* concentration following extraction by 90% acetone (Strickland and Parsons, 1972; Gong et al., 1993; Gong et al., 1995).

Water samples for  $\text{CH}_4$  concentration were collected in 120 mL dark borosilicate serum bottles. The bottles were rinsed three times with the sampled water. After a 2-fold bottle volume was allowed to overflow the bottle, 0.2 mL saturated  $\text{HgCl}_2$  was added. It was then sealed with a butyl stopper and crimped with an aluminum cap. The samples were stored in a dark box and kept at  $4^\circ\text{C}$ . All the water samples were transferred to a laboratory and analyzed within three months of collection. Measurements were made with the headspace technique (Weiss, 1981) and a gas chromatograph (GC; Agilent 7890) with a flame ionization detector (FID). The GC-FID had a 1.8 m

long stainless steel column with a diameter of 3.2 mm, which was filled with a 60/80 mesh molecular sieve 5A. The FID was calibrated with pure  $\text{N}_2$  (Yeong Her, Taiwan) and three commercial gas mixtures with  $\text{CH}_4$  mixing ratios of 1.16 ppmv (MESA Specialty Gas, USA), 3.02 ppmv (Yeong Her, Taiwan) and 9.60 ppmv (Yeong Her, Taiwan).

## $\text{CH}_4$ Saturation Ratio and Fluxes

The saturation ( $R$ , %) and sea-to-air flux ( $F$ ,  $\mu\text{mol}\cdot\text{m}^{-2}\cdot\text{d}^{-1}$ ) of  $\text{CH}_4$  were calculated using the following formulas:

$$R = (C_{obs}/C_{eq}) * 100$$

$$F (\mu\text{mol m}^{-2} \text{d}^{-1}) = k(C_{obs} - C_{eq})$$

$C_{obs}$  represents the observed concentration of gas dissolved in water, and  $C_{eq}$  is the expected equilibrium water concentration. The expected equilibrium water concentration was calculated using the solubility equation of (Wiesenburg and Norman, 1979), together with the *in situ* temperature, salinity and molar fraction of  $\text{CH}_4$  in the air. The atmospheric  $\text{CH}_4$  concentrations were taken from the NOAA/ESRL *in situ* program (<http://www.esrl.noaa.gov/gmd>). The monthly average atmospheric  $\text{CH}_4$  concentrations at Mauna Loa (Hawaii, United States station) in November, 2019, May 2020, August 2020 and December 2020 were 1900, 1901, 1878 and 1912 ppb, respectively. (The data for Jan. 2021 have not yet come out; therefore, December 2020 monthly average atmospheric  $\text{CH}_4$  concentrations were used).

Fluxes ( $\mu\text{mol}\cdot\text{m}^{-2}\cdot\text{d}^{-1}$ ) of  $\text{CH}_4$  across the air-water interface were determined by  $C_{obs}-C_{eq}$  and the gas exchange coefficient  $k$ . The value of  $k$  is a specific function of the properties of the gas, the temperature ( $^\circ\text{C}$ ) and turbulence and is frequently parameterized as a function of the wind speed. In this study, wind speed at a height of approximately 15 m above the sea

surface from a meteorological platform (121.3758°E 25.1817°N; **Figure 1**) was used. Daily wind speed data were provided by the Harbor and Marine Technology Center (<https://www.ihmt.gov.tw/>). We calculated  $k$  by using the equation established by Wanninkhof (2014). A positive flux indicates gas transfer from the water to the atmosphere.

## RESULTS

Marine hydrographic and chemical data as well as Chl  $a$  and CH<sub>4</sub> were measured during four seasonal cruises in the Tamsui River estuary adjacent marine area. Detailed information on the seasonal cruises and the average hydrographic data, nutrient concentrations, and Chl  $a$  and CH<sub>4</sub> concentrations are listed in **Table 1**. **Figure 2** presents cross-sectional studies of the Tamsui River estuary adjacent marine area in autumn, spring and summer.

### Marine Environmental Conditions and Methane Concentrations in the Dry Season (Autumn and Winter)

In autumn, the seawater temperature and salinity ranged from 18.9 to 24.0°C and 33.45 to 34.30 (**Table 1**), respectively. The seawater temperature gradually decreased with depth (**Figure 2A**), and the lowest salinity values were observed near shore (**Figure 2B**). The PO<sub>4</sub><sup>3-</sup> and NO<sub>3</sub><sup>-</sup> concentrations ranged from 0.26 to 0.78 μM and 2.9 to 9.4 μM (**Table 1**), respectively. The nutrient concentrations increased with depth and from offshore to inshore (**Figures 2C, D**). Chl  $a$  concentrations ranged between 0.15 and 1.50 mg m<sup>-3</sup> (**Table 1**) and gradient descent from the surface water (**Figure 2E**). DO concentrations ranged between 186.7 and 228.9 μM (**Table 1**) and had the same pattern as the Chl  $a$  distributions (**Figure 2F**). CH<sub>4</sub> concentrations ranged from 1.4 to 78.0 nM (**Table 1**), and high CH<sub>4</sub> concentrations were observed near station 11, where the outlet of the ocean outfall pipe which discharged the WWTP effluents was located (**Figure 2G**). The average surface seawater CH<sub>4</sub> concentration was 13.7 ± 18.7 nM. Long-term wind speed data from the meteorological platform were used, and the average wind speed in November between 2005 and 2019 was 7.9 ± 0.8 m/s. The sea-to-air CH<sub>4</sub> flux was 46.3 ± 75.4 μmol m<sup>-2</sup> d<sup>-1</sup> (**Table 2**).

In winter, only surface water was taken between stations 5 and 9 so there was no cross-sectional figure due to the adverse

weather conditions caused by the prevailing northeast monsoon. According to the data from 10 sampling stations, the seawater temperature and salinity ranged from 18.4 to 19.4°C and 33.06 to 34.35 (**Table 1**), respectively. Although nutrient concentrations were comparably high, with PO<sub>4</sub><sup>3-</sup> and NO<sub>3</sub><sup>-</sup> concentrations ranging from 0.44 to 0.85 μM and 6.0 to 8.5 μM, the Chl  $a$  concentrations were low, ranging between 0 and 0.30 mg m<sup>-3</sup> (**Table 1**). DO concentrations were comparably high and ranged between 227.7 and 252.4 μM (**Table 1**), which might be caused by low temperature and high wind ventilation. Wind speed data between 2005 and 2019 from the meteorological platform were used, and the average wind speed in January was 8.0 ± 0.8 m/s. CH<sub>4</sub> concentrations ranged from 5.4 to 69.6 nM, and the average surface CH<sub>4</sub> concentration was 27.0 ± 21.4 nM. With a comparably high wind speed, the sea-to-air CH<sub>4</sub> flux was as high as 90.4 ± 79.3 μmol m<sup>-2</sup> d<sup>-1</sup> (**Table 2**).

### Marine Environmental Conditions and Methane Concentrations in the Wet Season (Spring and Summer)

In spring, the seawater temperature and salinity ranged from 26.0 to 27.2°C and 31.68 to 34.46 (**Table 1**), respectively. The seawater temperature was homogeneous throughout the water column (**Figure 2H**). The PO<sub>4</sub><sup>3-</sup> and NO<sub>3</sub><sup>-</sup> concentrations ranged from 0.12 to 0.87 μM and 0 to 3.7 μM (**Table 1**), respectively. Low salinity and high nutrient concentrations were observed in the surface water and near the shore (**Figures 2I–K**) due to heavy precipitation on the sampling date. Chl  $a$  concentrations ranged between 0 and 0.77 mg m<sup>-3</sup> (**Table 1**) and had higher concentrations nearshore (**Figure 2L**). DO concentrations ranged between 193.1 and 216.0 μM (**Table 1**) and had a similar pattern as the Chl  $a$  distributions (**Figure 2M**). CH<sub>4</sub> concentrations ranged from 4.3 to 77.4 nM (**Table 1**), and high CH<sub>4</sub> concentrations were observed near the shore (**Figure 2N**). The average surface seawater CH<sub>4</sub> concentration was comparably high at 29.3 ± 19.8 nM. The average wind speed in May 2005 and 2019 from the meteorological platform was 5.0 ± 0.6 m/s. The sea-to-air CH<sub>4</sub> flux was 47.2 ± 34.3 μmol m<sup>-2</sup> d<sup>-1</sup> (**Table 2**).

In summer, the seawater temperature and salinity ranged from 27.0 to 30.8°C and 33.62 to 34.20 (**Table 1**), respectively. The seawater temperature gradually decreased with depth (**Figure 2O**), and low salinity values were observed near shore (**Figure 2P**). The PO<sub>4</sub><sup>3-</sup> and NO<sub>3</sub><sup>-</sup> concentrations ranged from 0.09

**TABLE 1** | The seasonal average hydrographic data, nutrients, Chl  $a$  and CH<sub>4</sub> concentrations.

Sampling Date		Temperature (°C)	Salinity	CH <sub>4</sub> (nM)	DO (μM)	PO <sub>4</sub> <sup>3-</sup> (μM)	NO <sub>3</sub> <sup>-</sup> (μM)	DIN (μM)	Chl $a$ (mg m <sup>-3</sup> )
Autumn	Range	18.9-24.0	33.45-34.30	1.4-78.0	186.7-228.9	0.26-0.78	2.9-9.4	3.58-10.15	0.15-1.50
Nov. 2019	Mean	23.4 ± 0.9	33.72 ± 0.20	13.0 ± 16.6	217.7 ± 7.4	0.38 ± 0.10	4.3 ± 1.1	5.66 ± 1.51	0.72 ± 0.25
Spring	Range	26.0-27.2	31.68-34.46	4.3-77.4	193.1-216.0	0.12-0.87	0-3.7	0.50-17.33	0-0.77
May 2020	Mean	26.8 ± 0.2	34.14 ± 0.47	20.2 ± 16.7	206.1 ± 4.5	0.26 ± 0.14	0.6 ± 0.6	3.09 ± 2.64	0.36 ± 0.15
Summer	Range	27.0-30.8	33.62-34.20	5.0-58.5	185.0-209.4	0.09-0.49	0-4.7	0.52-6.76	0.15-1.6
Aug. 2020	Mean	29.6 ± 0.9	34.00 ± 0.14	17.5 ± 13.1	190.8 ± 4.6	0.26 ± 0.10	1.1 ± 0.9	3.01 ± 1.61	0.56 ± 0.29
Winter	Range	18.4-19.4	33.06-34.35	5.4-69.6	227.7-252.4	0.44-0.85	6.0-8.5	6.83-13.14	0-0.30
Jan. 2021	Mean	18.6 ± 0.3	34.06 ± 0.37	20.4 ± 13.8	224.7 ± 7.9	0.59 ± 0.08	6.8 ± 0.6	8.49 ± 1.37	0.12 ± 0.07

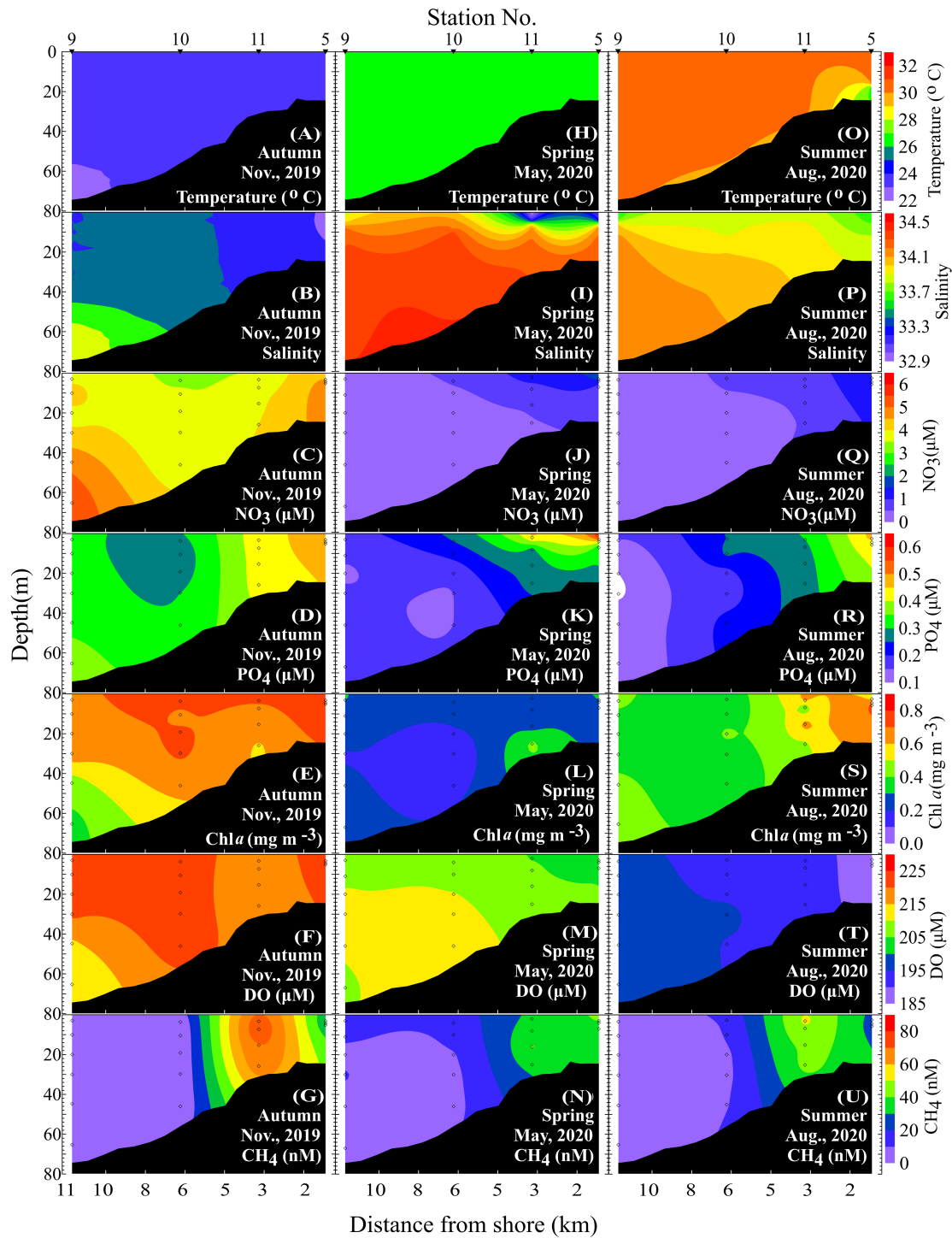


**FIGURE 2** | Cross-section of temperature, salinity, NO<sub>3</sub>, PO<sub>4</sub>, Chl *a*, DO and CH<sub>4</sub> (A–G) in autumn, (H–N) in spring, and (O–U) in summer.

to 0.49 μM and 0 to 4.7 μM (Table 1), respectively. Chl *a* and DO concentrations ranged from 0.15 to 1.60 mg m<sup>-3</sup> and 185.0 to 209.4 μM (Table 1), respectively. High nutrient and Chl *a* concentrations appeared nearshore (Figures 2Q–S) with low

salinity (Figure 2P), which indicated freshwater input from the shore. CH<sub>4</sub> concentrations ranged from 5.0 to 58.5 nM (Table 1), and high CH<sub>4</sub> concentrations were observed near the outlet of the ocean outfall pipe (Figure 2U). The average surface seawater

**TABLE 2** | The seasonal average surface hydrographic data, CH<sub>4</sub> concentrations, air CH<sub>4</sub> concentrations, wind speed and sea-to-air CH<sub>4</sub> fluxes.

Season	Sampling Date	Temperature (°C)	Salinity	Air CH <sub>4</sub> concentrations (ppm)	surface CH <sub>4</sub> concentrations (nM)	CH <sub>4</sub> saturation (%)	Monthly wind speed (m s <sup>-1</sup> )	Sea-to-air CH <sub>4</sub> fluxes (μmol m <sup>-2</sup> d <sup>-1</sup> )
Autumn	Nov. 2019	23.8 ± 0.2	33.63 ± 0.10	1.90 ± 0.01 <sup>a</sup>	13.7 ± 18.7	615 ± 840	7.9 ± 0.8	46.3 ± 75.4
Spring	May 2020	26.8 ± 0.2	33.71 ± 0.78	1.90 ± 0.02 <sup>a</sup>	29.3 ± 19.8	1383 ± 930	5.0 ± 0.6	47.2 ± 34.3
Summer	Aug. 2020	29.9 ± 0.7	33.89 ± 0.16	1.88 ± 0.01 <sup>a</sup>	21.8 ± 13.9	1095 ± 702	5.0 ± 0.7	37.0 ± 26.2
Winter	Jan. 2021	18.8 ± 0.4	33.75 ± 0.53	1.91 ± 0.02 <sup>a</sup>	27.0 ± 21.4	1104 ± 878	8.0 ± 0.8	90.4 ± 79.3

<sup>a</sup>Air CH<sub>4</sub> concentrations were from the monthly average data at Mauna Loa, Hawaii, United States.

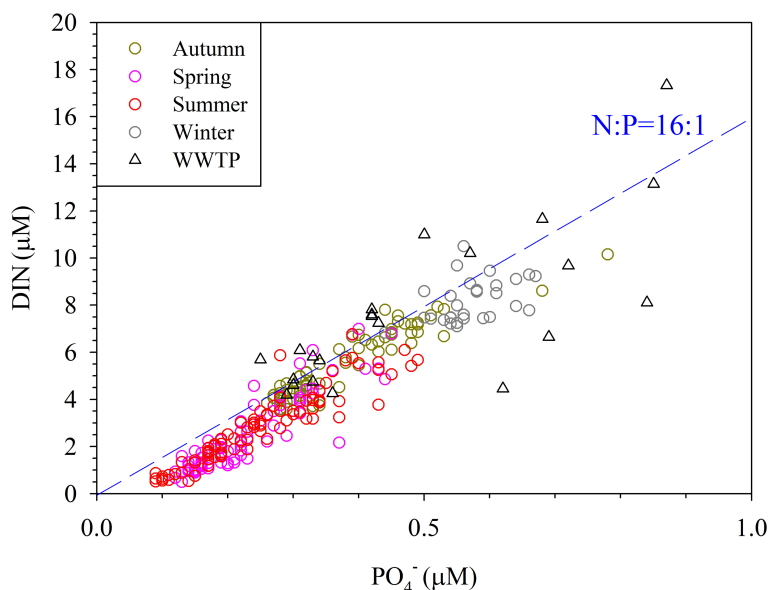


**FIGURE 3** | The DIN concentration (μM) versus PO<sub>4</sub> concentration (μM), obtained at 66 stations during four cruises from November 2019 to January 2021. Δ presents the data influenced by ocean outfall pipe of wastewater treatment plant.

CH<sub>4</sub> concentration was 21.8 ± 13.9 nM. The average wind speed in August between 2005 and 2019 from the meteorological platform was 5.0 ± 0.7 m/s. The sea-to-air CH<sub>4</sub> flux was 37.0 ± 26.2 μmol m<sup>-2</sup> d<sup>-1</sup> (**Table 2**).

## DISCUSSION

One of the effective options for mitigating rapid climate change is to reduce CH<sub>4</sub> emissions due to its shorter lifetime than CO<sub>2</sub> (Shindell et al., 2012), which leads to an urgent need to understand the natural or anthropogenic factors influencing CH<sub>4</sub> concentrations and emissions. The aim of this research is to understand the seasonal variations and possible sources of CH<sub>4</sub> concentrations as well as their interaction with other environmental factors in a populous urban coastal sea area.

### Inputs from WWTP Effluents

Wastewater is a major anthropogenic source of CH<sub>4</sub> and one of the fastest growing sources of CH<sub>4</sub> emissions (Kirschke et al., 2013).

According to the IPCC (2013), the wastewater CH<sub>4</sub> emissions from 2000 to 2009 represented 22.7% of all anthropogenic CH<sub>4</sub> emissions. Du et al. (2018) reported that CH<sub>4</sub> emissions from wastewater in China increased from 1349.01 Gg in 2000 to 3430.03 Gg in 2014, and the highest proportion of emissions was from WWTPs. Cotovicz et al. (2016) found that high CH<sub>4</sub> concentrations could be sustained by allochthonous sources, such as sewage networks and polluted rivers, especially under high accumulated precipitation conditions. Yu et al. (2017) also pointed out that high CH<sub>4</sub> concentrations are frequently found in the water of urban drainage systems, composed of sewer systems, and WWTPs. According to **Figure 2**, CH<sub>4</sub> concentrations were high from the bottom to the surface water near station 11, where the outlet of the ocean outfall pipe of the WWTP was located. In addition, most of the water samples near the ocean outfall pipe of the WWTP did not follow the Redfield ratio (**Figure 3**) and were high in surface CH<sub>4</sub> concentrations (**Figure 4**). Moreover, the highest CH<sub>4</sub> concentrations in the water column were found near the ocean outfall pipe of the WWTP (**Figures 2G, N, U**). The inputs from WWTP effluents contributed to the increase in the CH<sub>4</sub>

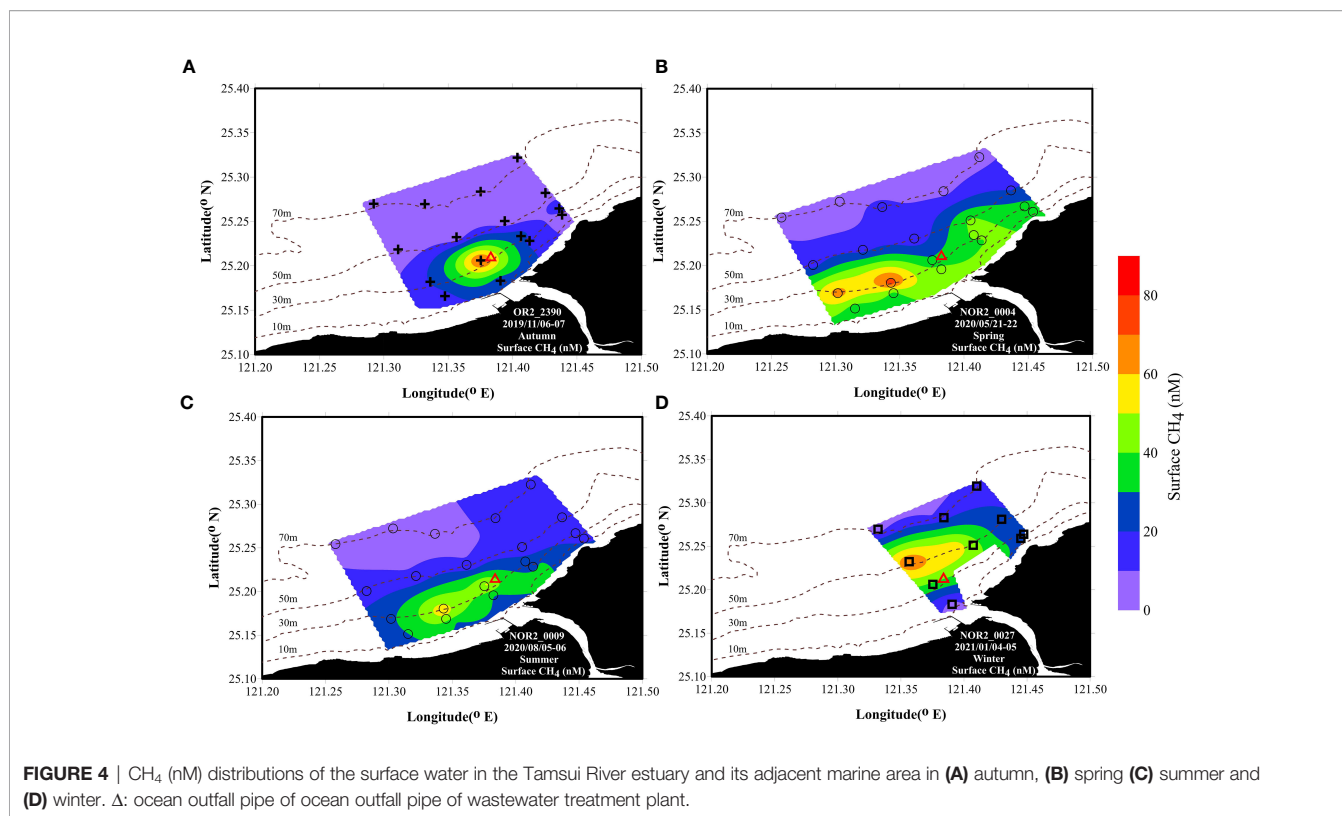


**FIGURE 4** | CH<sub>4</sub> (nM) distributions of the surface water in the Tamsui River estuary and its adjacent marine area in (A) autumn, (B) spring (C) summer and (D) winter. Δ: ocean outfall pipe of ocean outfall pipe of wastewater treatment plant.

concentrations in the study area. The average seasonal surface CH<sub>4</sub> concentrations were  $13.7 \pm 18.7$ ,  $29.3 \pm 19.8$ ,  $21.8 \pm 13.9$  and  $27.0 \pm 21.4$  nM in autumn, spring, summer and winter, respectively. If water samples near the ocean outfall pipe of the WWTP were excluded, the average seasonal surface CH<sub>4</sub> concentrations then became  $9.6 \pm 8.9$ ,  $21.5 \pm 13.2$ ,  $18.0 \pm 8.2$  and  $15.4 \pm 9.1$  nM in autumn, spring, summer and winter, respectively. This finding shows that approximately 17–43% of the surface CH<sub>4</sub> concentrations in the study area were influenced by the WWTP effluents. The average annual sea-to-air CH<sub>4</sub> flux was  $56.5 \pm 22.3$   $\mu\text{mol m}^{-2} \text{d}^{-1}$  and reached  $35.2 \pm 8.4$   $\mu\text{mol m}^{-2} \text{d}^{-1}$  when excluding the water samples near the ocean outfall pipe of the WWTP. This result indicated that WWTP effluents influenced approximately one-third of the CH<sub>4</sub> emissions in the study area.

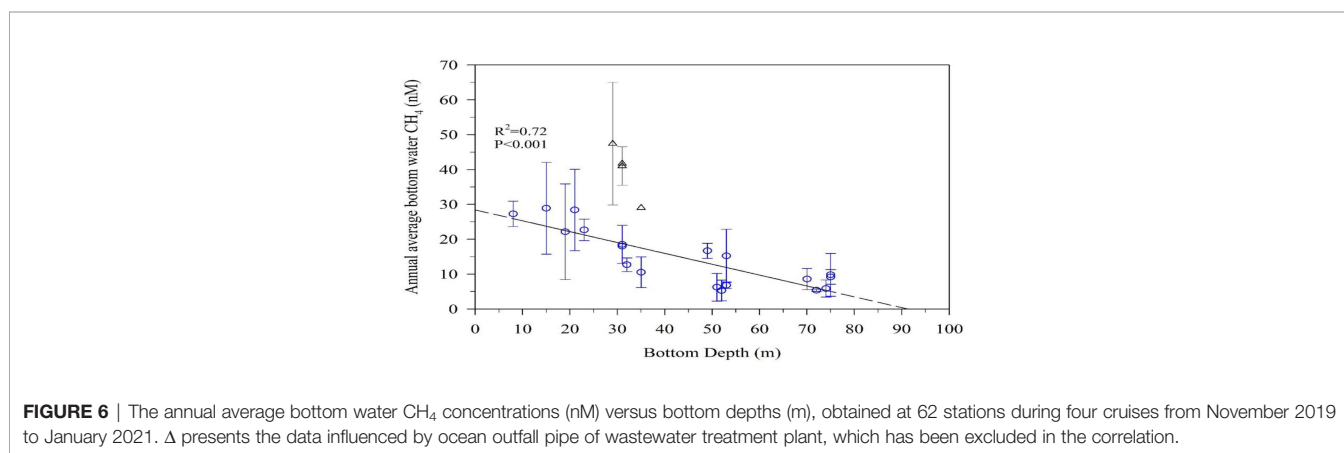
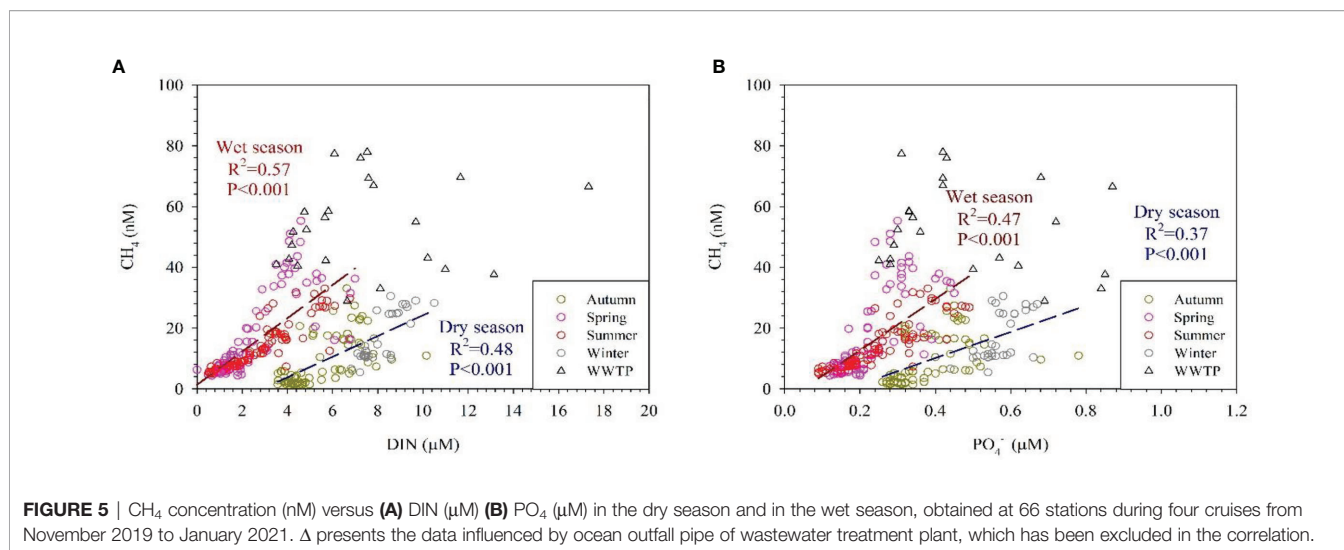
## Inputs From Freshwater

In addition to the inputs from WWTP effluents, freshwater also contributed to the CH<sub>4</sub> concentrations in the Tamsui River estuary adjacent marine area. The Tamsui River is a small mountain river with an average flow rate of approximately 210 m<sup>3</sup>/s. Although the Tamsui River transferred a comparably small amount of water mass to its adjacent marine areas, it brought high concentrations of CH<sub>4</sub> and nutrients. **Figure 2** shows high concentrations of CH<sub>4</sub> and nutrients with slightly low salinity nearshore. Dissolved inorganic nitrogen (DIN) concentrations represented the nitrogen level in the water and were well correlated with CH<sub>4</sub> concentrations (**Figure 5A**). CH<sub>4</sub> and PO<sub>4</sub><sup>3-</sup> concentrations also showed a positive correlation (**Figure 5B**). According to Nijman et al.

(2021), nutrients increased methane-oxidizing bacterial (MOB) abundance and methane oxidation potential, while warming only increased MOB abundance without altering methane oxidation potential. Thus, the differences of seawater temperature might result in different linear regressions between wet and dry seasons (**Figures 5A, B**).

## CH<sub>4</sub> Emissions From Sediment

Seasonal variations of CH<sub>4</sub> concentration in the Tamsui River ranged between 362 and 2961 nM (unpublished data). Rivers brought high concentrations of CH<sub>4</sub> and organic matter to coastal water (Chen et al., 2008; Zhang et al., 2008; Tseng et al., 2017; Sun et al., 2018). Coastal sediment which is rich in organic matter has been proposed to be the origin of CH<sub>4</sub> (Borges and Abril, 2011; Tseng et al., 2017). In addition, high CH<sub>4</sub> concentrations are frequently attributed to sedimentary methanogenesis in coastal environments (Bange, 2006; Zhou et al., 2009), especially in shallower waters. Borges et al. (2018) also found a seasonal peak of CH<sub>4</sub> in the nearshore and shallow seep areas in the Belgian coastal zone during summer, which was related to sediment organic matter content. **Figure 6** shows that CH<sub>4</sub> concentrations in the bottom water gradually decreased with the bottom depth. This result might be related to low abundance of methanotrophs in shallow coastal zones so more CH<sub>4</sub> seeps escaping from the sediment and higher CH<sub>4</sub> concentrations in the bottom water (Broman et al., 2020). According to our results, the CH<sub>4</sub> concentration in the bottom water did not influenced by the sediment input when the depth



deeper than 90m. This might be due to  $\text{CH}_4$  oxidized in the sediment before it released to the bottom water. According to the Sewerage Systems Office of the Public Works Department of the Taipei City Government, the ocean outfall pipe of a WWTP extends from shore, and its diffuser tubes are at water depths between 30 m and 40 m. Samples in the bottom water near the diffuser tubes were high in  $\text{CH}_4$  concentrations (Figure 6).

### Seasonal Variations in $\text{CH}_4$ and Sea-to-Air $\text{CH}_4$ Fluxes

Except for four individual observations in autumn, the surface water was supersaturated in  $\text{CH}_4$  with respect to the atmosphere at most stations in the Tamsui River estuary adjacent marine area during the four cruises, which indicated that the study area was a net source of atmospheric  $\text{CH}_4$ . The average surface seawater  $\text{CH}_4$  concentration varied between 13.7 and 29.3 nM (Table 2). The average surface seawater  $\text{CH}_4$  concentrations were higher in spring, summer and winter (29.3, 21.8 and 27.0 nM) and lower in autumn (13.7 nM). In spring

and summer (wet seasons), river discharge was more due to high precipitation and brought high concentrations of nutrients and  $\text{CH}_4$  from land to sea. In addition, relatively strong vertical mixing and disturbances might bring high  $\text{CH}_4$  concentrations from the bottom to the surface water in winter.

Figure 7 shows the average 15-year (2005-2019) monthly wind speed from the meteorological platform. In autumn, low river discharge and the wind speed was just picking up after October so the vertical mixing was relatively weak comparing with that in winter, which resulted in the lowest average surface seawater  $\text{CH}_4$  concentrations. The wind speeds were higher in autumn and winter than in spring and summer (Table 2). The sea-to-air  $\text{CH}_4$  flux variability was within the range of  $-3.0$ – $308.9 \mu\text{mol m}^{-2} \text{d}^{-1}$ . The average sea-to-air  $\text{CH}_4$  flux was the highest in winter ( $90.4 \mu\text{mol m}^{-2} \text{d}^{-1}$ ), followed by spring and autumn ( $47.2$  and  $46.3 \mu\text{mol m}^{-2} \text{d}^{-1}$ ) and was lowest in summer ( $37.0 \mu\text{mol m}^{-2} \text{d}^{-1}$ ).

When compared globally, the Scheldt estuary in the North Sea has the highest surface  $\text{CH}_4$  concentrations in its adjacent marine area, followed by the Tamsui River, Changjiang, and

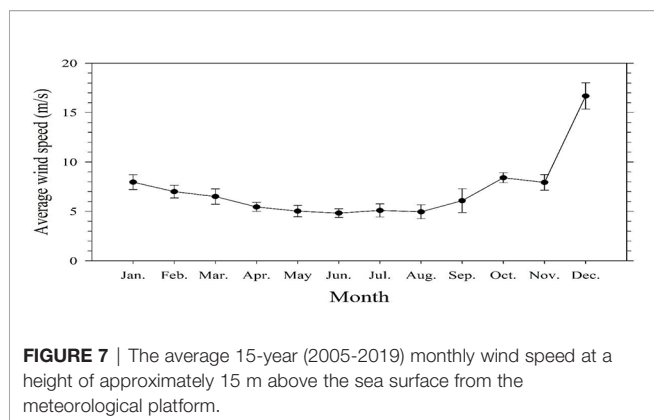


**FIGURE 7** | The average 15-year (2005-2019) monthly wind speed at a height of approximately 15 m above the sea surface from the meteorological platform.

Pearl River (Table 3). In regard to the sea-to-air  $\text{CH}_4$  fluxes, the adjacent marine areas of Scheldt and Tamsui River are the highest. Extremely high  $\text{CH}_4$  was observed near the Scheldt estuary adjacent marine area due to gassy sediments (Borges et al., 2016), and its emission may be increased when the ocean warms (Borges et al., 2018). Furthermore, inputs from WWTP effluents increased  $\text{CH}_4$  concentrations in the Tamsui River estuary adjacent marine area, and this situation may be worsened when the population grows.

## CONCLUSIONS

In this study, we characterized the spatial distribution and seasonal variations in  $\text{CH}_4$  in the Tamsui River estuary adjacent marine area as well as estimated sea-to-air  $\text{CH}_4$  fluxes to quantify the strength of the study area as an atmospheric  $\text{CH}_4$  source. The Tamsui River estuary adjacent marine area were active sites for  $\text{CH}_4$  emissions. Our research results showed that  $\text{CH}_4$  concentrations in coastal areas were influenced by WWTP effluents, sediment and freshwater inputs. In addition,  $\text{CH}_4$  concentrations increased with the nutrient levels. Moreover, strong vertical mixing and disturbances might also increase  $\text{CH}_4$  emissions, especially in coastal areas.

Climate change may increase precipitation in tropical/subtropical areas and transfer more nutrients and organic matter from land to ocean. Extreme weather events, such as typhoons and cyclones, can increase  $\text{CH}_4$  emissions in coastal areas due to sediment disturbance. Anthropogenic conditions, such as high coastal populations, sewage, and WWTP effluents, also influence coastal  $\text{CH}_4$  emissions. Escalating a feedback loop continues to circle between greenhouse gas emissions and climate change might increase extreme weather events. Nevertheless, preventing unthinkable events from happening takes tremendous time and effort. Accelerating the process from the root through scientific

**TABLE 3** | Compilation of surface  $\text{CH}_4$  concentrations, saturations and fluxes from the several estuaries and their adjacent marine areas.

Area	Regional Sea	Sampling Date	n	Salinity	$\text{CH}_4$ concentrations (nM)	$\text{CH}_4$ saturation (%)	Wind speed ( $\text{m s}^{-1}$ )	Sea-to-air $\text{CH}_4$ fluxes ( $\mu\text{mol m}^{-2} \text{d}^{-1}$ )	References
Scheldt estuary adjacent marine area	North sea	2016 monthly	108	30.5-34.2	$47.4 \pm 44.5$		$5.5 \pm 2.1^a$	$60 \pm 112^e$	Borges et al., 2018
		May 2011	8	S<30	$12.6 \pm 8.1$	$505 \pm 323$	$5.0 \pm 3.6^b$	$20.2 \pm 22.7^f$	
		Aug. 2011	18		$10.4 \pm 7.7$	$480 \pm 356$	$5.8 \pm 1.7^b$	$21.7 \pm 28.0^f$	
		Oct. 2011	2		$8.9 \pm 6.5$	$371 \pm 264$	$7.1 \pm 2.3^b$	$27.5 \pm 33.6^f$	
Changjiang estuary and its adjacent marine area	East China Sea	Mar. 2011	36	S>30	$4.6 \pm 4.4$	$161 \pm 149$	$7.6 \pm 3.8^b$	$4.33 \pm 8.86^f$	Sun et al., 2018
		May 2011	37		$5.2 \pm 4.4$	$218 \pm 179$	$8.4 \pm 3.9^b$	$13.4 \pm 28.6^f$	
		Aug. 2011	16		$6.0 \pm 1.8$	$289 \pm 90$	$6.2 \pm 1.5^b$	$11.6 \pm 7.57^f$	
		Oct. 2011	31		$4.7 \pm 1.1$	$216 \pm 48$	$7.4 \pm 3.0^b$	$10.7 \pm 8.26^f$	
Pearl River estuary adjacent marine area	South China Sea	Dec. 2011	29		$4.3 \pm 1.2$	$174 \pm 41$	$8.7 \pm 2.8^b$	$9.34 \pm 7.96^f$	
		May 2002	18	S>30	$5.05 \pm 2.49$	$216 \pm 101$	$4.9 \pm 1.8^b$	$5.8 \pm 7.3^e$	
		June 2006	10		$6.22 \pm 3.52$	$289 \pm 180$	$6.8^c$	$18.1 \pm 17.1^e$	Zhang et al., 2008
		Aug. 2005	5		$6.85 \pm 3.77$	$348 \pm 187$	$7.6^c$	$26.2 \pm 23.1^e$	
		Oct. 2006	24		$7.09 \pm 3.62$	$350 \pm 179$	$5.9 \pm 2.5^b$	$14.4 \pm 12.0^e$	
		Nov. 2002	12		$3.53 \pm 0.68$	$161 \pm 32$	$7.6^c$	$7.3 \pm 3.8^e$	
Tamsui River estuary adjacent marine area	Taiwan Strait	Sep. 2003	22	$33.68 \pm 0.24$	$4.4 \pm 2.2$	$233 \pm 115$	$6.73^d$	$8.3 \pm 7.2^f$	Tseng et al., 2017
		Jul. 2005	19	$32.54 \pm 1.35$	$6.2 \pm 1.5$	$323 \pm 75$	$6.73^d$	$14.5 \pm 4.9^f$	
		Nov. 2019	16	$33.63 \pm 0.10$	$13.7 \pm 18.7$	$615 \pm 840$	$7.9 \pm 0.8^c$	$46.3 \pm 75.4^f$	
Tamsui River estuary adjacent marine area	Taiwan Strait	May 2020	20	$33.71 \pm 0.78$	$29.3 \pm 19.8$	$1383 \pm 930$	$5.0 \pm 0.6^c$	$47.2 \pm 34.3^f$	This study
		Aug. 2020	20	$33.89 \pm 0.16$	$21.8 \pm 13.9$	$1095 \pm 702$	$5.0 \pm 0.7^c$	$37.0 \pm 26.2^f$	
		Jan. 2021	10	$33.75 \pm 0.53$	$27.0 \pm 21.4$	$1104 \pm 878$	$8.0 \pm 0.8^c$	$90.4 \pm 79.3^f$	

<sup>a</sup>Wind speed from the Westhinder Platform in the Belgian Coastal Zone.

<sup>b</sup>Wind speed from the ship based in situ wind speeds.

<sup>c</sup>Averaged monthly wind speeds obtained from the weather monitoring station.

<sup>d</sup>Average monthly wind speeds were from the National Aeronautics and Space Administration (NASA) QuikSCAT satellite platform.

<sup>e</sup>Fluxes were calculated by Wanninkhof (1992) equation.

<sup>f</sup>Fluxes were calculated by Wanninkhof (2014) equation.

findings that identifying possible CH<sub>4</sub> sources is the pivotal information required to mitigate the crisis in time.

## DATA AVAILABILITY STATEMENT

The original contributions presented in the study are included in the article/supplementary material, further inquiries can be directed to the corresponding authors.

## AUTHOR CONTRIBUTIONS

H-CT and G-CG co-developed the idea of the study. H-CT led the research cruises and did the sampling. C-CL, H-JP, and YTYH did the sampling and data analysis. H-CT wrote the first draft of the article and all authors contributed equally

to the interpretation of the results and in writing the final manuscript.

## FUNDING

This research was supported by Ministry of Science and Technology of the ROC, Taiwan (MOST 108-2611-M-019-021-MY3).

## ACKNOWLEDGMENTS

The authors wish to thank the Ministry of Science and Technology of the ROC, Taiwan for supporting this research, and the captain and crews of Ocean Researcher 2 and New Ocean Researcher 2 for their assistance.

## REFERENCES

- Bange, H. W. (2006). Nitrous Oxide and Methane in European Coastal Waters. *Estuarine Coastal Shelf Sci.* 70, 361–374. doi: 10.1016/j.ecss.2006.05.042
- Bange, H. W., Bartell, U. H., Rapsomanikisa, S., and Andreae, M. O. (1994). Methane in the Baltic and North Seas and a Reassessment of the Marine Emissions of Methane. *Glob. Biogeochem. Cycles* 8, 465–480. doi: 10.1029/94GB02181
- Beaulieu, J. J., DelSontro, T., and Downing, J. A. (2019). Eutrophication Will Increase Methane Emissions From Lakes and Impoundments During the 21st Century. *Nat. Commun.* 10, 1375. doi: 10.1038/s41467-019-09100-5
- Bogard, M. J., del Giorgio, P. A., Boutet, L., Chaves, M. C. G., Prairie, Y. T., Merante, A., et al. (2014). Oxidic Water Column Methanogenesis as a Major Component of Aquatic CH<sub>4</sub> Fluxes. *Nat. Commun.* 5, 5350. doi: 10.1038/ncomms6350
- Borges, A. V., and Abril, G. (2011). “5.04 - Carbon Dioxide and Methane Dynamics in Estuaries,” in *Treatise on Estuarine and Coastal Science*. Eds. E. Wolanski and D. McLusky (Waltham: Academic Press), p. 119–161.
- Borges, A. V., Champenois, W., Gypens, N., Delille, B., and Harlay, J. (2016). Massive Marine Methane Emissions From Near-Shore Shallow Coastal Areas. *Sci. Rep.* 6, 27908. doi: 10.1038/srep27908
- Borges, A. V., Speeckaert, G., Champenois, W., Scranton, M. I., and Gypens, N. (2018). Productivity and Temperature as Drivers of Seasonal and Spatial Variations of Dissolved Methane in the Southern Bight of the North Sea. *Ecosystems* 21, 583–599. doi: 10.1007/s10021-017-0171-7
- Broman, E., Sun, X., Stranne, C., Salgado, M. G., Bonaglia, S., Geibel, M., et al. (2020). Low Abundance of Methanotrophs in Sediments of Shallow Boreal Coastal Zones With High Water Methane Concentrations. *Front. Microbiol.* 11, 1536. doi: 10.3389/fmicb.2020.01536
- Chen, C.-T. A., Wang, S.-L., Lu, X.-X., Zhang, S.-R., Lui, H.-K., Tseng, H.-C., et al. (2008). Hydrogeochemistry and Greenhouse Gases of the Pearl River, its Estuary and Beyond. *Quat. Int.* 186, 79–90. doi: 10.1016/j.quaint.2007.08.024
- Cotovicz, L. C., Knoppers, B. A., Brandini, N., Poirier, D., Costa Santos, S. J., and Abril, G. (2016). Spatio-Temporal Variability of Methane (CH<sub>4</sub>) Concentrations and Diffusive Fluxes From a Tropical Coastal Embayment Surrounded by a Large Urban Area (Guanabara Bay, Rio De Janeiro, Brazil). *Limnol. Oceanogr.* 61, S238–S252. doi: 10.1002/lno.10298
- Damm, E., Helmke, E., Thoms, S., Schauer, U., Nøthig, E., Bakker, K., et al. (2010). Methane Production in Aerobic Oligotrophic Surface Water in the Central Arctic Ocean. *Biogeosciences* 7, 1099–1108. doi: 10.5194/bg-7-1099-2010
- de Angelis, M. A., and Lee, C. (1994). Methane Production During Zooplankton Grazing on Marine Phytoplankton. *Limnol. Oceanogr.* 39 (6), 1298–1308. doi: 10.4319/lno.1994.39.6.1298
- Du, M., Zhu, Q., Wang, X., Li, P., Yang, B., Chen, H., et al. (2018). Estimates and Predictions of Methane Emissions From Wastewater in China From 2000 to 2020. *Earth's Future* 6, 252–263. doi: 10.1002/2017EF000673
- Etminan, M., Myhre, G., Highwood, E. J., and Shine, K. P. (2016). Radiative Forcing of Carbon Dioxide, Methane, and Nitrous Oxide: A Significant Revision of the Methane Radiative Forcing. *Geophys. Res. Lett.* 43. doi: 10.1002/2016GL071930
- Florez-Leiva, L., Damm, E., and Farias, L. (2013). Methane Production Induced by Dimethylsulfide in Surface Water of an Upwelling Ecosystem. *Prog. Oceanogr.* 112–113, 38–48. doi: 10.1016/j.pocean.2013.03.005
- Gelesh, L., Marshall, K., Boicourt, W., and Lapham, L. (2016). Methane Concentrations Increase in Bottom Waters During Summertime Anoxia in the Highly Eutrophic Estuary, Chesapeake Bay, U.S.A. *Limnol. Oceanogr.* 61, S253–S266. doi: 10.1002/lno.10272
- Gong, G. C., Chen, L. Y. L., and Liu, K. K. (1996). Chemical Hydrography and Chlorophyll a Distribution in the East China Sea in Summer: Implications in Nutrient Dynamics. *Cont. Shelf Res.* 16, 1561–1590. doi: 10.1016/0278-4343(96)00005-2
- Gong, G.-C., Shiah, F.-K., Liu, K.-K., Wen, Y.-H., and Liang, M.-H. (2000). Spatial and Temporal Variation of Chlorophyll a, Primary Productivity and Chemical Hydrography in the Southern East China Sea. *Cont. Shelf Res.* 20, 411–436. doi: 10.1016/S0278-4343(99)00079-5
- Gong, G.-C., Yang, W.-R., and Chang, J. (1995). *In Vivo* Fluorescence-Derived Chlorophyll a Concentrations in the Southern East China Sea. *Acta. Oceanogr. Taiwanica* 34, 73–85.
- Gong, G.-C., Yang, W.-R., and Wen, Y.-H. (1993). Correlation of Chlorophyll a Concentration and Sea Tech Fluorometer Fluorescence in Seawater. *Acta. Oceanogr. Taiwanica* 31, 117–126.
- Humborg, C., Geibel, M. C., Sun, X., McCrackin, M., Mörth, C.-M., Stranne, C., et al. (2019). High Emissions of Carbon Dioxide and Methane From the Coastal Baltic Sea at the End of a Summer Heat Wave. *Front. Marine Sci.* 6. doi: 10.3389/fmars.2019.00493
- IPCC (2013). Climate Change 2013: The Physical Science Basis. Contribution of Working Group I to the Fifth Assessment Report of the Intergovernmental Panel on Climate Change, in: T.F. Stocker, D. Qin, G.-K. Plattner, M. Tignor, S.K. Allen, J. Boschung, A. Nauels, et al. (Ed.), C.2; C.6; C.8, pp. 159–254; pp. 473–552; pp. 677–731. Cambridge, United Kingdom and New York, NY, USA.
- Jackson, R. B., Saunio, M., Bousquet, P., Canadell, J. G., Poulter, B., Stavert, A. R., et al. (2019). Increasing Anthropogenic Methane Emissions Arise Equally From Agricultural and Fossil Fuel Sources. *Environ. Res. Lett.* 15, 071002. doi: 10.1088/1748-9326/ab9ed2
- Karl, D. M., Beversdorf, L., Björkman, K. M., Church, M. J., Martinez, A., and Delong, E. F. (2008). Aerobic Production of Methane in the Sea. *Nat. Geosci.* 1, 473–478. doi: 10.1038/ngeo234
- Kirschke, S., Bousquet, P., Ciais, P., Saunio, M., Canadell, J. G., Dlugokencky, E. J., et al. (2013). Three Decades of Global Methane Sources and Sinks. *Nat. Geosci.* 6, 813–823. doi: 10.1038/ngeo1955
- Middelburg, J. J., Nieuwenhuize, J., Iversen, N., Høgh, N., Dewilde, H., Helder, W., et al. (2002). Methane Distribution in European Tidal Estuaries. *Biogeochemistry* 59, 95–119. doi: 10.1023/A:1015515130419

- Myllykangas, J.-P., Hietanen, S., and Jilbert, T. (2019). Legacy Effects of Eutrophication on Modern Methane Dynamics in a Boreal Estuary. *Estuaries Coasts* 43, 189–206. doi: 10.1007/s12237-019-00677-0
- Nijman, T. P. A., Davidson, T. A., Weideveld, S. T. J., Audet, J., Esposito, C., Levi, E. E., et al. (2021). Warming and Eutrophication Interactively Drive Changes in the Methane-Oxidizing Community of Shallow Lakes. *ISME Commun.* 1, 32. doi: 10.1038/s43705-021-00026-y
- Pai, S.-C., Gong, G.-C., and Liu, K.-K. (1993). Determination of Dissolved Oxygen in Seawater by Direct Spectrophotometry of Total Iodine. *Marine Chem.* 41, 343–351. doi: 10.1016/0304-4203(93)90266-Q
- Pekel, J. F., Cottam, A., Gorelick, N., and Belward, A. S. (2016). High-Resolution Mapping of Global Surface Water and Its Long-Term Changes. *Nature* 540, 418–422. doi: 10.1038/nature20584
- Reeburgh, W. S. (2007). Oceanic Methane Biogeochemistry. *Chem. Rev.* 107, 486–513.
- Rehder, G., Keir, R. S., Suess, E., and Pohlmann, T. (1998). The Multiple Sources and Patterns of Methane in North Sea Waters. *Aquat. Geochem.* 4, 403–427. doi: 10.1023/A:1009644600833
- Repeta, D. J., Ferrón, S., Sosa, O. A., Johnson, C. G., Repeta, L. D., Acker, M., et al. (2016). Marine Methane Paradox Explained by Bacterial Degradation of Dissolved Organic Matter. *Nat. Geosci.* 9, 884–887. doi: 10.1038/ngeo2837
- Rhee, T. S., Kettle, A. J., and Andreae, M. O. (2009). Methane and Nitrous Oxide Emissions From the Ocean: A Reassessment Using Basin-Wide Observations in the Atlantic. *J. Geophys. Res.* 114, D12304. doi: 10.1029/2008JD011662
- Shindell, D., Kuylenstierna, J. C., Vignati, E., van Dingenen, R., Amann, M., Klimont, Z., et al. (2012). Simultaneously Mitigating Near-Term Climate Change and Improving Human Health and Food Security. *Science* 335, 183–189. doi: 10.1126/science.1210026
- Strickland, J. D. H., and Parsons, T. R. (1972). *A Practical Handbook of Seawater Analysis* (Ottawa, Canada: Fisheries Research Board of Canada), p. 310.
- Sun, M. S., Zhang, G. L., Ma, X., Cao, X. P., Mao, X. Y., Li, J., et al. (2018). Dissolved Methane in the East China Sea: Distribution, Seasonal Variation and Emission. *Marine Chem.* 202, 12–26. doi: 10.1016/j.marchem.2018.03.001
- Tilbrook, B. D., and Karl, D. M. (1994). Dissolved Methane Distributions, Sources, and Sinks in the Western Bransfield Strait, Antarctica. *J. Geophys. Res.* 99, 16383–16393. doi: 10.1029/94JC01043
- Tseng, H.-C., Chen, C.-T. A., Borges, A. V., DelValls, T. A., and Chang, Y.-C. (2017). Methane in the South China Sea and the Western Philippine Sea. *Cont. Shelf Res.* 135, 23–34. doi: 10.1016/j.csr.2017.01.005
- Tseng, H.-C., Newton, A., Gong, G.-C., and Lin, C.-C. (2021). Social-Environmental Analysis of Estuary Water Quality in a Populous Urban Area. *Elem. Sci. Anth.* 9, 1. doi: 10.1525/elementa.2020.00085
- Upstill-Goddard, R. C., Barnes, J., Frost, T., Punshon, S., and Owens, N. J. P. (2000). Methane in the Southern North Sea: Low-Salinity Inputs, Estuarine Removal, and Atmospheric Flux. *Glob. Biogeochem. Cycles* 14, 1205–1217. doi: 10.1029/1999GB001236
- Wanninkhof, R. (1992). Relationship Between Wind Speed and Gas Exchange Over the Ocean. *J. Geophys. Res.* 97, 7373–7382. doi: 10.1029/92JC00188
- Wanninkhof, R. (2014). Relationship Between Wind Speed and Gas Exchange Over the Ocean Revisited. *Limnol. Oceanogr. Methods* 12, 351–362. doi: 10.4319/lom.2014.12.351
- Weiss, R. F. (1981). Determinations of Carbon Dioxide and Methane by Dual Catalyst Flame Ionization Chromatography and Nitrous Oxide by Electron Capture Chromatography. *J. Chromatogr. Sci.* 19, 611–616. doi: 10.1093/chromsci/19.12.611
- Wen, L.-S., Jiann, K.-T., and Liu, K.-K. (2008). Seasonal Variation and Flux of Dissolved Nutrients in the Danshuei Estuary, Taiwan: A Hypoxic Subtropical Mountain River. *Estuarine Coastal Shelf Sci.* 78, 694–704. doi: 10.1016/j.ecss.2008.02.011
- Wiesenburg, D. A., and Norman, L. G. J. (1979). Equilibrium Solubilities of Methane, Carbon Monoxide, and Hydrogen in Water and Sea Water. *J. Chem. Eng. Data* 24, 356–360. doi: 10.1021/je60083a006
- Yu, Z., Wang, D., Li, Y., Deng, H., Hu, B., Ye, M., et al. (2017). Carbon Dioxide and Methane Dynamics in a Human-Dominated Lowland Coastal River Network (Shanghai, China). *J. Geophys. Res.: Biogeosci.* 122, 1738–1758. doi: 10.1002/2017JG003798
- Yvon-Durocher, G., Allen, A. P., Bastviken, D., Conrad, R., Gudas, C., St-Pierre, A., et al. (2014). Methane Fluxes Show Consistent Temperature Dependence Across Microbial to Ecosystem Scales. *Nature* 507, 488–491. doi: 10.1038/nature13164
- Zhang, G., Zhang, J., Liu, S., Ren, J., Xu, J., and Zhang, F. (2008). Methane in the Changjiang (Yangtze River) Estuary and its Adjacent Marine Area: Riverine Input, Sediment Release and Atmospheric Fluxes. *Biogeochemistry* 91, 71–84. doi: 10.1007/s10533-008-9259-7
- Zhou, H., Yin, X., Yang, Q., Wang, H., Wu, Z., and Bao, S. (2009). Distribution, Source and Flux of Methane in the Western Pearl River Estuary and Northern South China Sea. *Marine Chem.* 117, 21–31. doi: 10.1016/j.marchem.2009.07.011
- Zindler, C., Bracher, A., Marandino, C. A., Taylor, B., Torrecilla, E., Kock, A., et al. (2013). Sulphur Compounds, Methane, and Phytoplankton: Interactions Along a North-South Transit in the Western Pacific Ocean. *Biogeosciences* 10, 3297–3311. doi: 10.5194/bg-10-3297-2013

**Conflict of Interest:** The authors declare that the research was conducted in the absence of any commercial or financial relationships that could be construed as a potential conflict of interest.

**Publisher's Note:** All claims expressed in this article are solely those of the authors and do not necessarily represent those of their affiliated organizations, or those of the publisher, the editors and the reviewers. Any product that may be evaluated in this article, or claim that may be made by its manufacturer, is not guaranteed or endorsed by the publisher.

Copyright © 2022 Tseng, Lin, Pan, Han and Gong. This is an open-access article distributed under the terms of the Creative Commons Attribution License (CC BY). The use, distribution or reproduction in other forums is permitted, provided the original author(s) and the copyright owner(s) are credited and that the original publication in this journal is cited, in accordance with accepted academic practice. No use, distribution or reproduction is permitted which does not comply with these terms.